WSRC-TR-98-00290 (U)

Preliminary Report on the Dissolution Rate and Degradation of Aluminum Spent Nuclear Fuels in Repository Environments (U)

B. J. Wiersma
Savannah River Technology Center
Strategic Materials Department
Materials Technology Section

J. I. Mickalonis
Savannah River Technology Center
Strategic Materials Department
Materials Technology Section

Publication Date: August 1998

Westinghouse Savannah River
Savannah River Site
Aiken, SC 29808

This document was prepared in connection with work done under Contract No. DE-AC09-89SR18035 with the U. S. Department of Energy. By acceptance of this document, the publisher and/or recipient acknowledges the U. S. Government's right to retain a nonexclusive, royalty-free license in and to any copyright covering this document, along with the right to reproduce and authorize others to reproduce all or part of the copyrighted material.

Legacy - NO
(Savannah River Rept)

DISCLAIMER

This report was prepared as an account of work sponsored by an agency of the United States Government. Neither the United States Government nor any agency thereof, nor any of their employees, makes any warranty, express or implied, or assumes any legal liability or responsibility for the accuracy, completeness, or usefulness of any information, apparatus, product, or process disclosed, or represents that its use would not infringe privately owned rights. Reference herein to any specific commercial product, process, or service by trade name, trademark, manufacturer, or otherwise does not necessarily constitute or imply its endorsement, recommendation, or favoring by the United States Government or any agency thereof. The views and opinions of authors expressed herein do not necessarily state or reflect those of the United States Government or any agency thereof.

WSRC-TR-98-00290 (U)

SMTD
Strategic Materials Technology Department

Keywords: Corrosion, Radionuclide Release Rate

Retention - Permanent

Preliminary Report on the Dissolution Rate and Degradation of Aluminum Spent Nuclear Fuels in Repository Environments (U)

by

B. J. Wiersma

J. I. Mickalonis

DOES NOT CONTAIN UNCLASSIFIED CONTROLLED NUCLEAR INFORMATION

ADC & Reviewing Official: D. Thomas Rabi

Date: August 28, 1998

SRTC SAVANNAH RIVER TECHNOLOGY CENTER, AIKEN, SC 29808
Westinghouse Savannah River Company
Prepared for the U. S. Department of Energy under Contract DE-AC09-89SR18035

APPROVALS

Bruce J. Wiersma — Date: 8/27/98

B. J. Wiersma, Author
Materials Applications & Corrosion Technology Group
MATERIALS TECHNOLOGY SECTION

P. E. Zapp — Date: 8-26-98

P. E. Zapp, Technical Reviewer
Materials Applications & Corrosion Technology Group
MATERIALS TECHNOLOGY SECTION

Nathan Iyer — Date: 8/27/98

N. C. Iyer, Manager
Materials Applications & Corrosion Technology Group
MATERIALS TECHNOLOGY SECTION

S. L. West for T. L. Capeletti — Date: 8/31/98

T. L. Capeletti, Manager
MATERIALS TECHNOLOGY SECTION

W F Swift — Date: 8/27/98

W. F. Swift, Manager
SPENT FUEL STORAGE DIVISION

TABLE OF CONTENTS

I. INTRODUCTION AND SUMMARY 1
II. EXPERIMENTAL PROCEDURE 2
Single-Pass Flow Test 2
Static Test 3
Electrochemical Tests 4
Al-SNF Test Samples Characterization 4
Irradiated Al-SNF Samples 5
Unirradiated U-Al Alloy Samples 6
Test Solutions 6
III. EXPERIMENTAL RESULTS 7
Irradiated Al-SNF Samples 8
J-13 Well Water 8
Nitric Acid 9
Bicarbonate 10
Unirradiated U-Al Alloy Samples 10
19 UAl Alloy 10
10, 13.2, And 25 UAl Alloy 11
Static Test Results 16
Corrosion Mechanism of U-Al Alloys 16
Analysis of Test Solutions Dissolved Species 20
Corrosion Losses of U-Al Alloys 23
Electrochemical Test Results 23
IV. DISCUSSION 23
Uranium Dissolution Rates and Radionuclide Release Rate 26
Effect of Degradation Mechanism on the Uranium Dissolution Rate 26
Degradation Mechanism 26
Effects of Environmental Variables on the Dissolution and Degradation of Al-SNF 27
V. CONCLUSIONS 28
VI. ACKNOWLEDGEMENTS 29
VII. REFERENCES 29

LIST OF FIGURES

Figure 1. PNNL Flow Test Set-Up 2
Figure 2. SRS Flow Test Cell 3
Figure 3. Schematic of Static Test Apparatus 4
Figure 4. Photomicrographs of Al-SNF: a) UAl_x, b) UAl, c) U_3O_8, d) U_3Si_2 5
Figure 5. Microstructures of U-Al Test Samples: a) 10 UAl cast, b) 13.2 UAl cast, c) 25 UAl cast, d) 13.2 UAl wrought 7
Figure 6. UAl Dissolution Rate in Nominal J-13 at 25 °C 9
Figure 7. UAl Dissolution Rate in the Nitric Acid Solution at 25 °C 9
Figure 8. UAl Dissolution Rate in the Bicarbonate Solution at 25 °C 10
Figure 9. 19 UAl Microstructure: A) Before Test, B) After Test in Nominal J-13, C) After Test in Nitric Acid Solution, D) After Test in Bicarbonate Solution 11
Figure 10. U Dissolution Rates for 13.2 UAl Cast Coupons in J-13 Waters at 90 °C 13
Figure 11. Al Dissolution Rates for 13.2 UAl Cast Coupons in J-13 Waters at 90 °C 13
Figure 12. U Dissolution Rates for 13.2 UAl Cast Coupons in J-13 Waters at 25 °C 13
Figure 13. Al Dissolution Rates for 13.2 and 25 UAl Cast Coupons in Low pH J-13 at 25 °C 14
Figure 14. Planar View of Surface Of 25 UAl Cast In Nominal J-13 15
Figure 15. Cross-section of 25 UAl Cast in Low pH J-13 15
Figure 16. Post-test Microstructure of 13.2 UAl Cast from Nominal J-13 at 90°C 16
Figure 17. SEM Micrograph of Dislodged U-Al Particles from 25 UAl Wrought in High pH J-13 at 90°C 17
Figure 18. Post-test Microstructure of 13.2 UAl Cast from Low pH J-13 at 90°C 17
Figure 19. Cross-sectional View of Post-test Microstructure of 13.2 UAl Cast from Low pH J-13 at 90°C 17
Figure 20. Post-test Microstructure of 13.2 UAl Cast from High Cl J-13 at 90°C 18
Figure 21. Post-test Microstructure of 13.2 UAl Cast from High pH J-13 at 90°C 18
Figure 22. Cross-sectional View of Post-test Microstructure of 25 UAl Cast from Nominal J-13 at 90°C 19
Figure 23. Cross-sectional View of Post-test Microstructure of 13.2 UAl Wrought from Low pH J-13 at 90°C 19
Figure 24. Visual Appearance of 13.2 UAl Cast from High Cl J-13 at 90°C and Coupled to a) Stainless Steel and b) Aluminum (2X) 20
Figure 25. Post-test Surface of Crevice Area of 13.2 UAl Wrought from Nominal J-13 at 90°C 20
Figure 26. The Polarization Curve for 13.2 UAl in Nominal J-13 at 90 °C 24
Figure 27. The Polarization Curve for 10 UAl in High pH J-13 at 25 °C 25

LIST OF TABLES

Table 1. Radionuclide Content of Irradiated Al-SNF 6
Table 2. Solution Composition of Nominal J-13 Well Water 8
Table 3. Uranium Dissolution Rates ($mgU/m^2/d$) 8
Table 4. Average Uranium and Aluminum Dissolution Rates ($mg/m^2/d$) from Flow Tests 12
Table 5. Weight Changes of U-Al Alloys in J-13 Waters 15
Table 6. Concentration (ppm) of Dissolved Uranium in Static Tests at 90°C: a) Stainless Steel and b) Aluminum 21
Table 7. Concentration (ppm) of Dissolved Uranium for 13.2 UAl Cast Material Couple to Stainless Steel in Static Tests as a Function of Temperature 21
Table 8. Concentration (ppm) of Dissolved Aluminum in Static Tests at 90 °C: a) Stainless Steel and b) Aluminum 22
Table 9. Concentration (ppm) of Dissolved Aluminum for 13.2 UAl Cast Material Coupled to Stainless Steel in Static Tests as a Function of Temperature 23
Table 10. Weight Changes ($\mu g/dm^2$) in Coupons from Static Tests of 13.2 UAl Cast at 90°C for Stainless Steel and Aluminum Galvanic Couples 23
Table 11. Weight Changes ($\mu g/dm^2$) in 13.2 UAl Cast Coupons Coupled to Stainless Steel in Static Tests as a Function of Temperature 23
Table 12. Corrosion Potentials and Rates for Cast U-Al Alloys in J-13 Waters 25

I. INTRODUCTION AND SUMMARY

The Department of Energy (DOE) is pursuing several options for the disposition of aluminum-based spent nuclear fuel (Al-SNF). Two such options are either the direct disposal of the present fuel form or the melt/dilute option in which the Al-SNF is recast as forms with lower uranium enrichment. The performance of Al-SNF in the repository will differ from that of the commercial nuclear fuels and the high level waste glasses. The Al-SNF is less stable and more reactive than the other waste forms, in part due to the aluminum cladding. This cladding may also be susceptible to galvanic corrosion with the canister material. The fuel meat of the Al-SNF, which has a two-phase structure, is more highly enriched than commercial fuels. Characterization of the various spent fuels is required prior to acceptance for the repository. Therefore, the environmental degradation of the Al-SNF and their release of radionuclides are of concern.

Single pass flow tests were utilized to measure dissolution rates of radionuclides from the Al-SNF. Development of this database will provide a preliminary input to the performance assessment and the materials redistribution and reconfiguration analysis that will address criticality concerns. Tests were performed on four irradiated fuel types: UAl, UAl_X, U_3O_8, and U_3Si_2. Unirradiated UAl alloys ranging from 10 to 25 wt % U were also tested. The variables were the solution chemistry, which were variants of J-13 well water (J-13), temperature (25 and 90 °C), alloy composition of the fuel, and alloy fabrication technique. The nominal J-13 composition was based on a water chemistry from a well near the Yucca Mountain repository excavation site. The irradiated fuels had dissolution rates at 25 °C that ranged from approximately 0.2 $mgU/m^2/day$ ($mgU/m^2/d$) for all the fuels in nominal J-13 to 30-100 $mgU/m^2/d$ in a nitric acid solution. Dissolution rates for radionuclides such as Cs, Sr, and Pu were approximately the same as the U dissolution rate over the duration of the test. However, Tc dissolution rates showed a large degree of variability and did not always coincide with the U dissolution rates. The unirradiated alloys had dissolution rates ranging from 0.2 $mgU/m^2/d$ in nominal J-13 at 25 °C to 200-400 $mgU/m^2/d$ in low pH J-13 at 90 °C.

Along with the flow tests, static coupon and electrochemical tests were also performed on the unirradiated alloys to discern the effects of material degradation mechanism on the U dissolution rate. The results from all three tests showed that the test environment, which included aqueous phase chemistry and temperature, had the greatest effect. The effects on the dissolution were minimal for the alloy composition and fabrication. The type of galvanic couple when made with the alloys in the static test also increased the U dissolution. The degradation was observed to follow a two-stage process. During the initial stage, preferential corrosion of the aluminum matrix adjacent to the U-Al particles occurred regardless of the environmental variables. During the second stage, an oxide film generally formed on the surface of the coupon. The alloys were also susceptible to pitting in these environments.

The oxide thickness, which depended on the solution chemistry, temperature, and flow condition, affected the U dissolution. The oxide was thick for a low pH J-13 (pH~3) and undetectable for the high pH J-13 (pH~11). In the saturated condition with the low pH J-13, the thick oxide prevented further U dissolution, but not in the unsaturated condition. The U solubility restricted dissolution in the high pH J-13 for both conditions. In the nominal and high Cl J-13, a thin oxide film deposited, protecting the surface of the coupon and minimizing U dissolution. Pitting, which occurred in both the nominal and high Cl J-13, did not affect the U dissolution rate in the chloride range tested.

In addition to solution chemistry, the effects of other experimental variables such as temperature and type of galvanic couple were also investigated. In solutions where a thin oxide or no oxide formed (i.e., nominal, high Cl, and high pH J-13), the U dissolution rate increased with temperature. However, when a thick oxide was formed (i.e., low pH J-13) the U dissolution rate was insensitive to temperature. The effect of galvanic coupling was tested only in the static tests, where a stainless steel galvanic couple resulted in an increase in the degradation and dissolution rate in all solutions.

II. EXPERIMENTAL PROCEDURE

Single-pass flow tests were used to measure the dissolution rates of radionuclides from Al-SNF. Static coupon and electrochemical tests were also performed to assess the effects of material degradation on the U dissolution rate. The test variables included the solution chemistry, which were variants of J-13, temperature, alloy composition of the fuel, alloy fabrication technique and type of galvanic coupling.

Single-Pass Flow Test

The flow test was configured to measure the dissolution rates of radionuclides. These single pass flow tests maintained the uranium concentration below the solubility limits thereby allowing the forward rate of reaction of the fuel with the water to be measured. Flow tests had been used previously to study the dissolution of commercial nuclear fuels [1,2]. The primary flow test parameters were fuel composition, water chemistry, and temperature. For the Al-SNF, two different flow test apparatuses were used, but each maintained the conditions of single pass and low flow rates.

Flow tests were performed at Pacific Northwest National Laboratory (PNNL) in stainless steel systems where the water was mechanically pumped [3]. The test apparatus is shown schematically in Figure 1. Reciprocating plunger, positive displacement pumps pulsed the water at an average flow rate of 12 mL/h. The water was fed in an upward flow through the test cell. The test cell, 12 mm ID x 51 mm long, were made of stainless steel and capped at the ends by stainless steel frits. The cells were fitted with glass sleeves to prevent galvanic interaction between the cell and test coupons. Each cell contained one coupon. The test cell and waste water container were inside a hot-cell for testing the irradiated samples. Unirradiated coupons were tested outside a hot cell. All tests were conducted at ambient temperature, ~25°C, and atmospheric oxygen conditions.

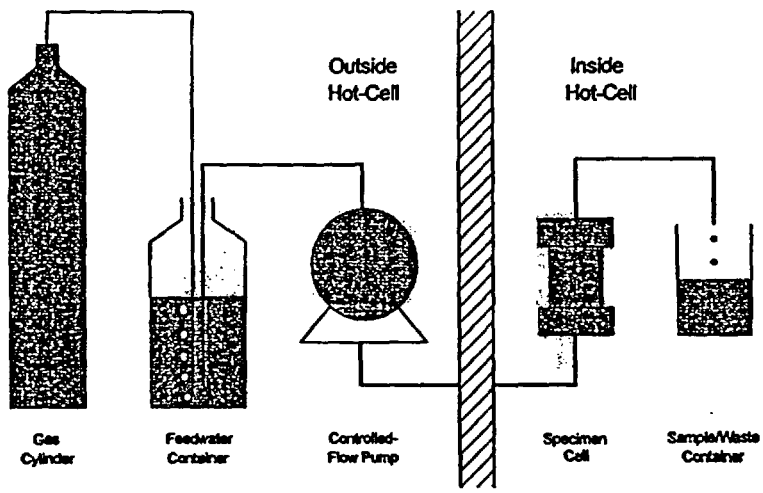

Figure 1. PNNL Flow Test Set-Up

Test samples were prepared by cutting coupons from either irradiated or unirradiated fuel. For the irradiated coupons, the aluminum cladding (0.38 t 0.81 mm thick) was ground off one side. All the coupons, 12 mm by 25 mm, were polished to 1-μm surface finish. The geometric surface areas of the polished faces were ~2.8 cm^2 and of the unpolished edges of exposed fuel meat were 0.2 to 0.4 cm^2 except for the U-Al alloy, which was ~1.4 cm^2. All six surfaces of the unirradiated fuel were exposed fuel meat. Geometric surface areas of the polished faces were ~5.5 cm^2 and of the unpolished edges ~3.0 cm^2.

Two different systems were used at SRS to control the flow rate, although both were similar to the PNNL design. As stated previously all flow apparatuses were single pass and low flow. One system was a gravity feed. The flow initiated from a feed reservoir which fed four cells simultaneously through individual

metered stopcocks. The stopcocks were adjusted to control the flow in a range of 10-15 ml/hr. The second drive system was similar to the PNNL design and used mechanical pumps. The pumps maintained the flow rate at a more constant level. From the stopcock, the water dripped into a feed line for each cell. For the pumps, tygon tubing was used from the pump to the feed line.

As shown in Figure 2, the water flowed into the feed line and through the bottom of the flow cell, discharging from the top of the cell. The test cell was made from borosilicate glass and did not have filters since the samples were monoliths. Four coupons were in each cell and separated by a glass support tree. The cell was 12.7mm ID and 63.5 mm long. Samples were taken each week for chemical analysis of uranium, aluminum, and the other primary constituents of the solution. Tests were conducted at room temperature and 90 °C.

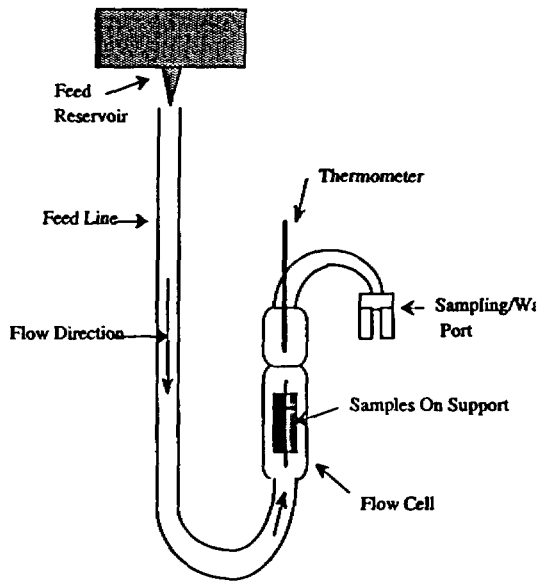

Figure 2. SRS Flow Test Cell

The samples, which had the dimensions of 0.25 in. × 0.25 in. × 0.5 in., were exposed for 2-3 months. Surfaces were initially prepared with a 1000 grit finish. After testing, representative samples were examined using light and electron microscopy to characterize the corrosion morphology. Samples were also weighed to monitor weight changes resulting from corrosion or oxidation.

Static Test

For the static tests, the procedures and apparatus were developed from ASTM G31-71 [3]. The test apparatus consisted of a 2.5 L glass vessel, heating mantle, and temperature controller. The static tests were conducted so that the U-Al samples were coupled to either a stainless steel or aluminum plate for investigating galvanic and crevice corrosion. Figure 3 shows a schematic of the test apparatus. Temperatures of 25 and 90 °C were used.

The samples were bolted to the plates with nylon hardware, which passed through a central hole drilled through the sample. The samples were 0.5-inch cubes with surfaces ground to a 1000 grit finish. Pre- and post- test characterization, including optical metallography and SEM, were performed for each sample to detect changes in structure. Samples were also weighed to monitor weight changes resulting from corrosion or oxidation.

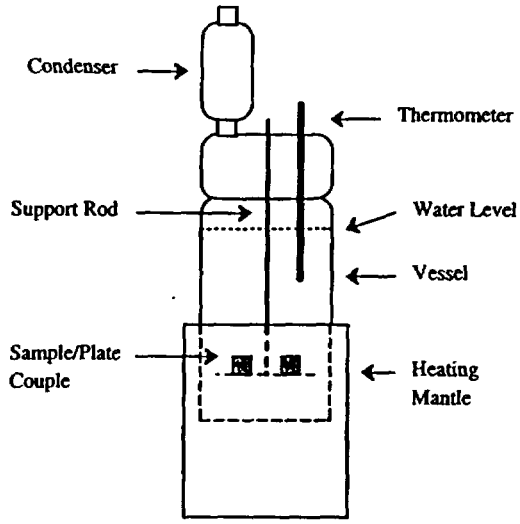

Figure 3. Schematic of Static Test Apparatus

The tests were performed for one month. Samples were removed from the vessel at intervals of 7, 14, and 28 days which provided data for the time dependence of the degradation rate. Solution samples were also taken to determine species dissolution. Chemical analyses included ICPES for Al and Chemcheck™ for uranium. After the test, the solution was filtered to remove any particulate that was subsequently analyzed using SEM and EDS.

Electrochemical Tests

The electrochemical tests included linear and cyclic potentiodynamic polarization. The test procedures were based on ASTM standards [5,6]. The electrochemical tests involved applying a potential to the sample and measuring the responding current. The current-potential relationship is a function of the active corrosion mechanism. Specific corrosion parameters and characteristics were determined from the data including the corrosion potential, a general corrosion rate (linear polarization resistance), and pitting susceptibility.

The tests were performed with an EG&G Princeton Applied Research Model 273 potentiostat under computer control. For the linear and cyclic tests, the samples were polarized from the natural or open-circuit potential at a rate of 0.2 mV/sec. The linear polarization was performed on the sample prior to the cyclic scan. The samples were placed into standard glass electrochemical cells after the solution had come to temperature. Test temperatures included room temperature and 95 °C. The counter electrodes were graphite rods and the reference electrode was a high temperature Ag/AgCl electrode. Air was bubbled slowly through the solution during the test.

The samples were 0.5 inch cubes which were mounted in a cold cure epoxy. The surface was polished to a 800 grit surface finish and cleaned prior to immersion. After the test, a sample was visually evaluated for corrosion morphology. Solution samples were taken after testing for chemical analysis.

Al-SNF Test Samples Characterization

The test samples for this study were both irradiated Al-SNF and unirradiated U-Al alloys. The irradiated fuel samples were prepared at Argonne National Laboratory. The unirradiated U-Al alloys were made at SRS.

Irradiated Al-SNF Samples

The irradiated samples for the PNNL flow test were sectioned from four irradiated Al-SNF each with a different fuel material. The fuel materials were U-Al, UAl_x-Al (x = 3 or 4), U_3O_8-Al, and U_3Si_2-Al. These plate-type fuels ranged in thickness from 1.3-4.1 mm. The aluminum cladding was removed to expose the actual fuel material. Photomicrographs of the four fuels are shown in Figure 4. The results with the samples with removed coating can be used to project the potential for release of radionuclides from a repository after the cladding has corroded away or in the event that the fuel is somehow physically damaged after emplacement.

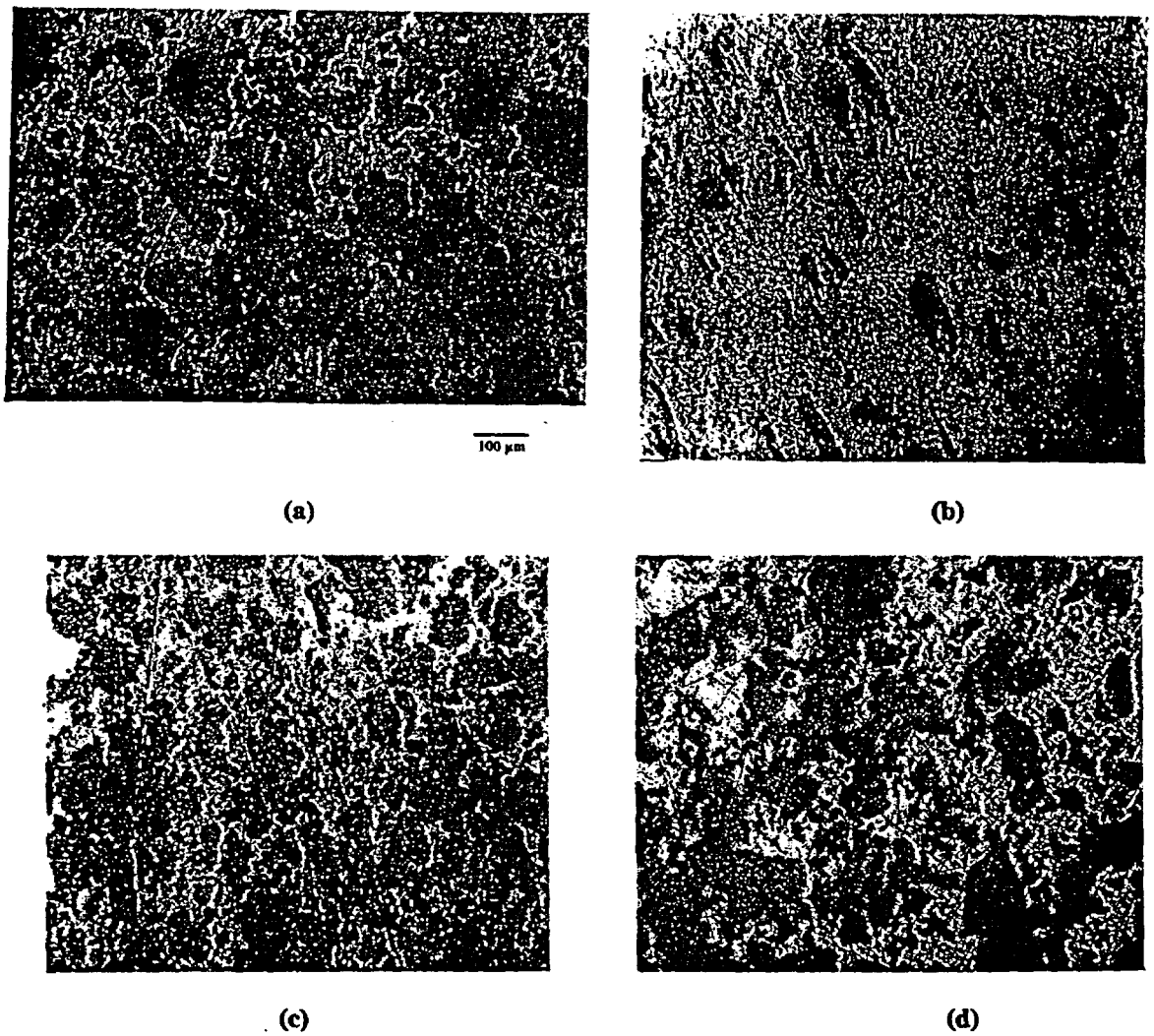

Figure 4. Photomicrographs of Al-SNF: a) UAl_X, b) UAl, c) U_3O_8, d) U_3Si_2

The radionuclides and quantities of U and Al in the irradiated test specimens were measured from three 0.1 g pieces cut from a coupon of each fuel type. The pieces were completely dissolved through the following steps: 6 M HCl to dissolve the aluminum and concentrated nitric to dissolve the fuel material. The U_3Si_2 fuel did not fully dissolve, so the residue was treated by fusing with KOH, and then dissolving in a mixture of HNO_3 and HCl. The solution analyses included U, Al, $^{239+240}Pu$, ^{238}Pu, ^{137}Cs, ^{99}Tc, and ^{90}Sr and the results are shown in Table 1. The listed analyses are for fuel meats and the aluminum matrix.

Table 1. Radionuclides Content of Irradiated Al-SNF*

Fuel	Enrich. (%^{235}U)	Burnup (%)	Al (g/g)	U (g/g)	$^{239+240}$Pu (mCi/gU)	^{238}Pu (mCi/gU)	^{137}Cs (mCi/gU)	^{99}Tc (mCi/gU)	^{90}Sr (mCi/gU)
UAl_x	45	73	0.750	0.138	1.83	21.7	1240	0.113	1010
UAl	80	40	0.763	0.144	0.61	28.8	1210	0.108	1050
U_3O_8	45	72	0.763	0.134	1.69	16.5	1140	0.106	960
U_3Si_2	20	93	0.387	0.449	1.26	15.5	500	0.040	410

* Activities of radionuclides are based on U content. The quantities for Al and U are based on total sample weight.

The table lists the averages of the triplicate analyses except for the UAl_x fuel where one of the three analyses differed somewhat from the other two and was not included in the average. Residue from the initial U_3Si_2 dissolution was found to be predominantly Si and, in particular, contained completely negligible amounts of the elements and radionuclides. The totals, obtained by adding the Al and original U quantities, were 95-100% of the weights of the analyses specimens. This high percentage was considered a good mass balance agreement.

Unirradiated U-Al Alloy Samples

In addition to the irradiated fuels, a range of U-Al alloys were also tested. The compositions were 10, 13.2 (eutectic), 19, and 25 wt % U with the balance aluminum (10 UAl, 13 UAl, 19 UAl, and 25 UAl). The 19 UAl sample was unirradiated version of the UAl fuel. This alloy was tested at both PNNL and SRS, while the remaining U-Al alloys were tested at SRS only.

The U-Al alloys were produced from a supply of bulk aluminum ingots (1100 Al) and depleted uranium. The materials were melted in an induction furnace between 800 and 1400 °C, depending on the alloy composition. The alloys were cast into molds and cooled in air. Metallographic analyses indicated that the microstructures were fairly uniform throughout the cross-section of the ingots. Several ingots of the 13.2 and 25 UAl alloys were extruded and rolled to produce a wrought structure. The wrought and cast structures were representative of either unprocessed or melt and diluted Al-SNF, respectively. Samples were cut from the ingots with either an electric discharge machine or a mill.

The surfaces of the coupons were examined with a scanning electron microscope (SEM) prior to initiating the tests. Figure 5 (a) shows a micrograph of the 10 UAl cast material. The dark area was the primary aluminum phase, while the light, skeletal areas are the eutectic phase. The eutectic consists of the lamellae of aluminum and the UAl_4 phase. The cast microstructure consists mostly of aluminum dendrites with eutectic filling the interdendritic regions. Figure5 (b) shows a micrograph of the 13.2 UAl cast material, the eutectic composition. A greater fraction of the surface is covered with eutectic than was observed for the 10 UAl cast. Additionally, a few light, blocky structures are present in the midst of the aluminum matrix. These blocky structures are the UAl_3 phase. Figure 5 (c) shows a micrograph of the 25 UAl cast material. The UAl_3 phase was much more apparent at this composition. Small regions of the eutectic phase were also seen. The diamond shape particles with the dark center (i.e., aluminum phase) are also the UAl_4 phase. Figure 5 (d) shows a micrograph of 13.2 UAl wrought material. Due to the rolling of the material the particles were crushed and are aligned in the rolling direction.

Test Solutions

The solutions for all the tests were based on the composition of water taken near a proposed repository site. Variations of the J-13 water were used to simulate various scenarios due to interactions with soils and other waste forms. The J-13 water with a pH of ~8 had a nominal composition similar to that of Beavers et al. [7]. For the PNNL flow tests two other water chemistries were used, 2×10^{-2} M $NaHCO_3$ at pH of 8, and nitric acid at pH of 3. Three other variants of J-13 were used for the remaining tests: low pH (~3), high pH (~11),

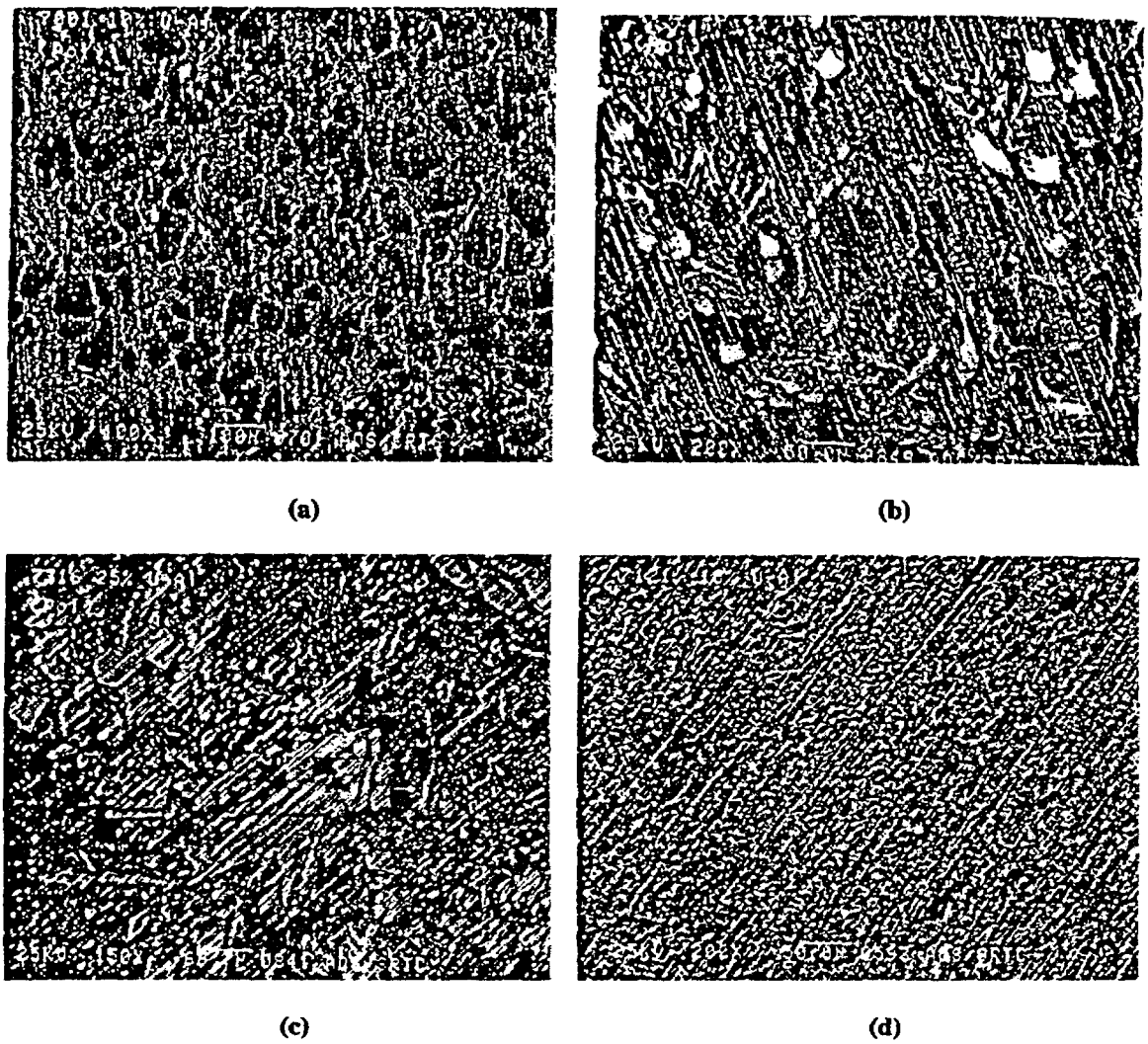

Figure 5. Microstructures of U-Al Test Samples: a) 10 UAl cast, b) 13.2 UAl cast, c) 25 UAl cast, d) 13.2 UAl wrought

and high chloride (60 ppm Cl^-). The low and high pH J-13 waters were made by additions of either nitric acid or sodium hydroxide, respectively. Additional sodium chloride was added to make the high Cl J-13. The conductivities of these J-13 waters ranged as follows: nominal J-13, 250-350 µS; low pH, 450-600 µS; high pH, 1200-7500 µS; high Cl, 400-450 µS.

Solution analyses were performed on small samples taken during the tests at various intervals to determine the dissolution and corrosion rates. For the irradiated coupons, 10 mL samples were collected initially twice a week and then approximately once each week. Samples were analyzed for the following elements and radionuclides: U, Al, $^{239+240}Pu$, ^{238}Pu, ^{137}Cs, ^{99}Tc, and ^{90}Sr. For the unirradiated coupons, sampling was similar, but analyses included only U and Al.

III. EXPERIMENTAL RESULTS

The preliminary dissolution rates of radionuclides from the enriched Al-SNF were based on the results of flow tests from both irradiated and unirradiated samples. In conjunction with this test, corrosion testing was

Table 2. Solution Composition of Nominal J-13 Well Water

Constituent	(ppm)	Constituent	(ppm)
Calcium	13	Chloride	7.1
Potassium	5.3	Fluoride	2.3
Magnesium	1.9	Nitrate	8.1
Sodium	44	Sulfate	18
Silicon	33	Carbonate	120

conducted using static, electrochemical, and galvanic tests to determine the effect of the degradation mechanism of Al-SNF on the dissolution rates of the radionuclides. The results from the different tests are presented in the following section.

Irradiated Al-SNF Samples

Dissolution rates for the irradiated samples were measured for not only the primary constituent uranium, but also for aluminum, cesium, plutonium, strontium, and technetium. The average dissolution rates for uranium from the different fuels are presented in Table 3 for the three test solutions, that is the J-13 well water simulant, nitric acid, and bicarbonate. The dissolution rate (DR) was calculated by the following equation:

$$DR = (C_i \times F) / SA ,$$

where C_i is the elemental concentration of either U or Al (ppm), F is the flow rate, 0.2 ml/min, and SA is the geometric surface area (m^2) of the sample exposed to the solution. The dissolution data, in general, were variable, so a standard averaging protocol was not used. The post-test metallographic characterization of the irradiated test coupons is being performed at Argonne National Laboratory.

Table 3. Uranium Dissolution Rates ($mgU/m^2/d$)

Fuel	J-13 Well Water	Nitric Acid	Bicarbonate
UAl_X	0.19	28	22
UAl	0.17	99	33
U_3O_8	0.14	31	33
U_3Si_2	0.22	36	36

J-13 Well Water

During the initial stages of the test in the J-13 well water, the water samples were found to be contaminated from uranium in the hot cell. The average dissolution rates for the radionuclides were based on the rates calculated between 50 and 209 days. As shown in Table 3, the U dissolution rates from the four fuels varied between 0.14 to 0.22 $mgU/m^2/d$. Figure 6 shows the UAl dissolution rate for J-13 at 25 °C over the course of the test. These dissolution rates, however, are normalized to a calculated surface area of the fuel meat exposed to the test solution, which for UAl was 31% of the geometric area. The Al concentration in the analysis sample was generally below the detection limit of 60 μg/L except for the first sample drawn at 12 days. The Al concentrations in the J-13 corresponded to a dissolution rate of 30-50 $mgAl/m^2/d$. Tc was not analyzed for the J-13 water because the low U concentrations indicated the Tc concentration would be below the detection limit. The other radionuclides varied for each of the fuels, but in general were similar or lower than that of uranium. The Cs and Sr dissolution rates for U_3Si_2 were the only exception and were higher than that of uranium.

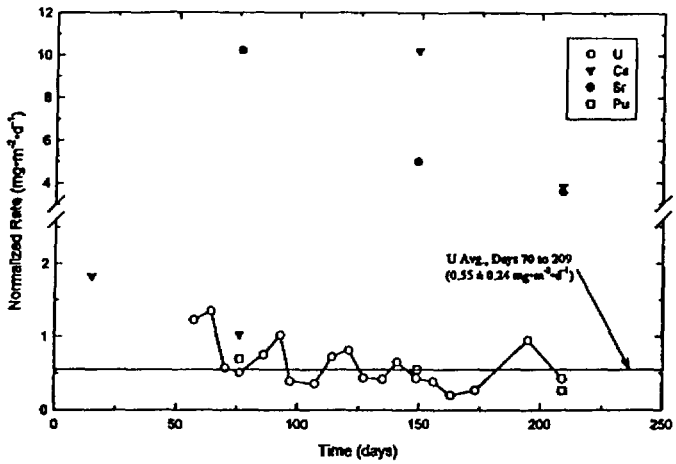

Figure 6. UAl Dissolution Rate in Nominal J-13 at 25 °C

Nitric Acid

The U dissolution rate in the nitric acid ranged between 28-99 mgU/m^2/d for the four fuels as shown in Table 3. The initial 8-day transients were not included in calculating the average. The data for the U_3O_8 sample were not stable for the first 44 days, so these were excluded from the average. The UAl coupon had the most variable data over the course of the 236-day test period as shown in Figure 7 and also had the highest average dissolution rate. The dissolution rates in the figure are normalized to a calculated surface area of the fuel meat exposed to the test solution, which for UAl was 31% of the geometric area. Aluminum, in the range of 1000 mgAl/m^2/d, dissolved faster than the uranium for all the fuels except for the UAl coupon. For UAl, the U and Al dissolution rates were similar. Cs and Sr dissolution rates from the fuels were also similar to that of uranium, except for U_3Si_2 where the rates were higher. The Pu dissolution rates were similar to that of uranium for all the fuels. The Tc concentrations were low and irregular, but sufficiently above the detection limit to negate analytical uncertainty. The Tc concentration also depended on the fuel. For example, with UAl_X the Tc data were congruent with the U data, whereas for the UAl fuel several points were abnormally high.

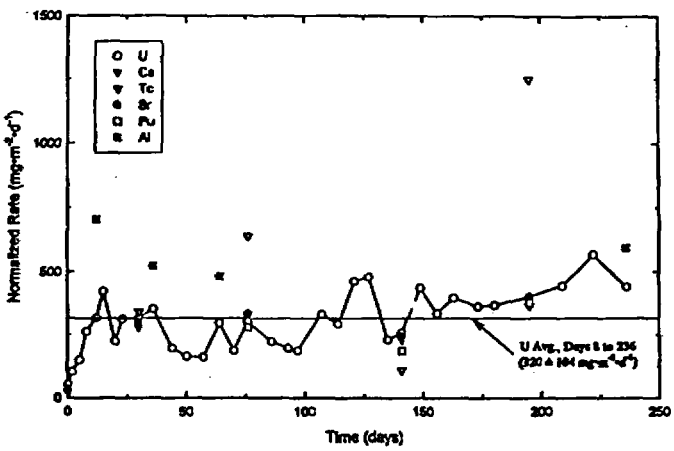

Figure 7. UAl Dissolution Rate in the Nitric Acid Solution at 25 °C

Bicarbonate

The measured U concentrations in the bicarbonate solution over the 222-day test period were more variable than in the other two solutions as shown in Figure 8 for the UAl fuel. The dissolution rates in the figure are normalized to a calculated surface area of the fuel meat exposed to the test solution, which for UAl was 31% of the geometric area. The stable data for the fuels also varied, although the U dissolution rates were fairly similar, ranging from 22 to 36 mgU/m^2/d as shown in Table 3. The U concentration dropped after 135 days for all but the U_3Si_2, which remained stable. Initially, the Al dissolution rate was higher than that of uranium, but then had similar rates for the remainder of the test. The Cs and Sr dissolution rates were similar to that of uranium, except for U_3Si_2 where the rates were higher. The Pu dissolution rates were lower than that of U for all the fuels and the Pu concentration was on the order of 10^{-9} mol/L. As for the nitric acid solution, the Tc dissolution rates were inconsistent and varied for all the fuels.

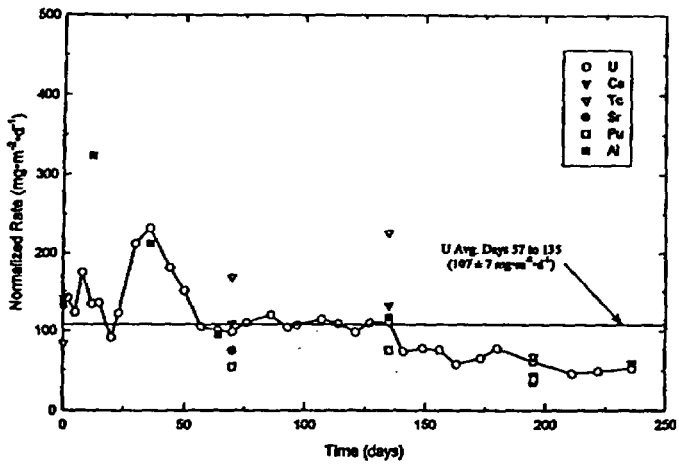

Figure 8. UAl Dissolution Rate in the Bicarbonate Solution at 25 °C

Unirradiated U-Al Alloy Samples

The unirradiated test samples were alloys with the following U concentrations: 10, 13.2, 19, and 25 wt %. The 19 UAl is discussed separately from the other alloys since its composition is similar to the irradiated U-Al fuel. Additionally, the other alloys were tested in variants of J-13 and not the nitric acid and bicarbonate solutions.

19 UAl Alloy

The dissolution rates of aluminum and uranium were measured in the same solutions as the irradiated coupons. For the J-13 water, the U dissolution rate was 0.2 mgU/m^2/d for the 113-day test. From the limited aluminum measurements, the Al dissolution rate appeared to be greater than that of uranium. In the nitric acid solution, the Al dissolution rate was also greater than the U dissolution rate, which was 230 mgAl/m^2/d. In the bicarbonate solution, however, the U and Al dissolution occurred at the same rate of 25 mg/m^2/d.

The microstructural characteristics of the alloy varied depending on the solution chemistry as shown in Figure 9 (a)-(d). In Figure 9 (a), which shows the untested coupon, the microstructure consisted of U-Al particles embedded in an Al matrix. After 113 days, the J-13 water had a minimal effect as shown in Figure 9 (b). In the nitric acid, both the matrix and U-Al particles were attacked as shown in Figure 9 (c). Since the aluminum dissolution was greater than that of the uranium, the U-Al particles typically protruded from the surface. The 19 UAl in the bicarbonate solution had a mud-cracked appearance typical of aluminum oxide. In Figure 9 (d), the coupon was washed to remove any dried salts.

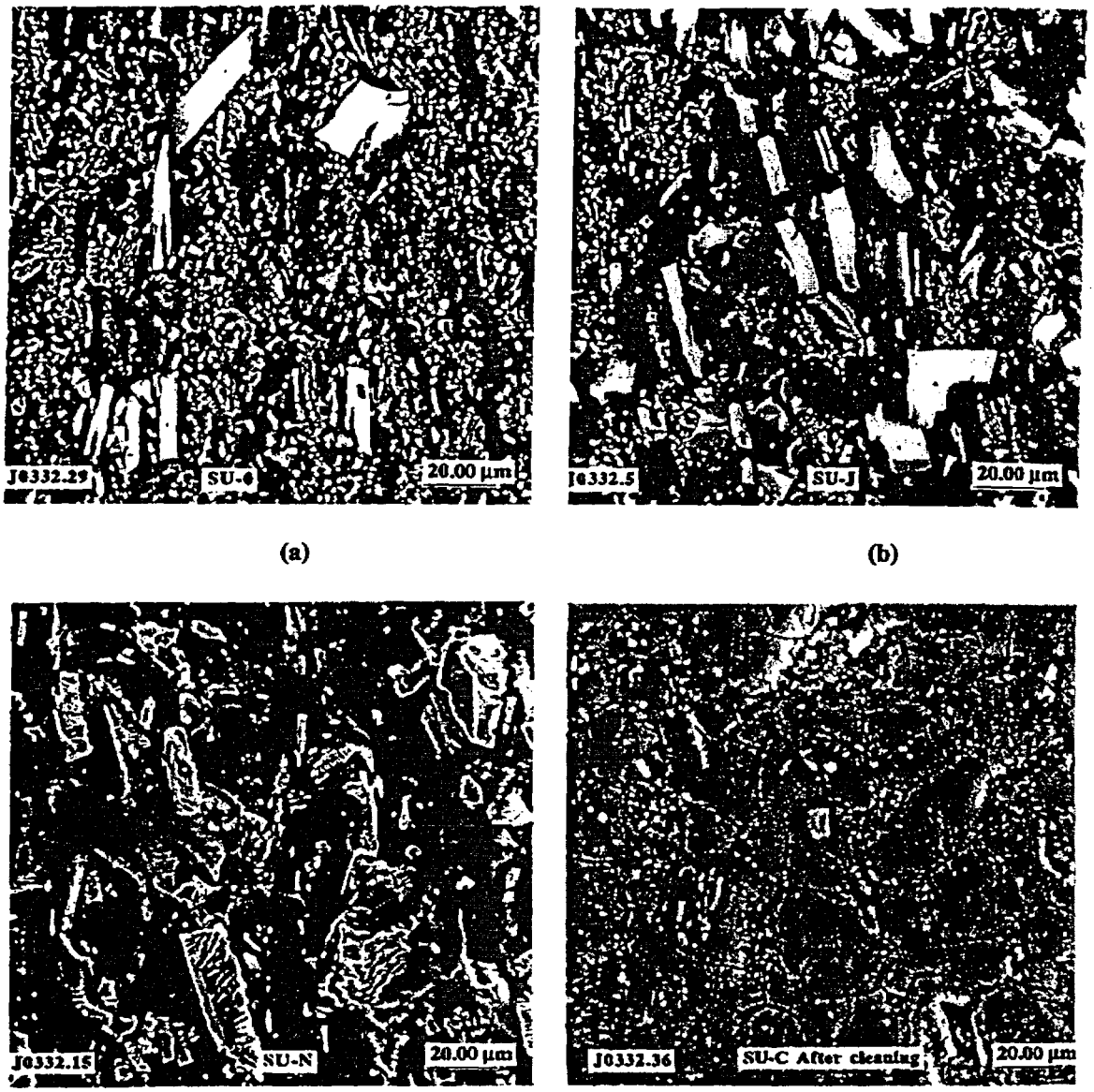

Figure 9. 19 UAl Microstructure: A) Before Test, B) After Test in Nominal J-13, C) After Test in Nitric Acid Solution, D) After Test in Bicarbonate Solution

A duplicate test was performed at SRS with another 19 UAl coupon to assess alloy variability. The U dissolution rate from this test was approximately 1.8 mgU/m^2/d, which was ten times greater than the first measurement. Some of the variability may have been associated with experimental error and differences in the test procedures. The variability is still being evaluated by characterization of surface preparation and analysis technique.

10, 13.2, And 25 UAl Alloy

The flow test for these unirradiated alloys was performed to measure U dissolution rates and to characterize Al-SNF degradation mechanisms and the effects of the fuel microstructure. The flow test results consisted of the dissolved U and Al concentrations, the visual and microscopic observations of the coupons, and the

weight changes of the alloys. The U dissolution rates were similar for the three alloys and were dependent primarily on the solution chemistry, temperature, and the subsequent corrosion mechanisms.

The U and Al dissolution rates are shown in Table 4 for the different alloys in each J-13 water chemistry at temperatures of 25 and 90 °C, although the data at 25 °C is limited. These average values were calculated from measured weekly concentrations and are not normalized to the initial elemental inventory. The U dissolution rate was always less than that for aluminum, generally by an order of magnitude. The elements reacted differently to the J-13 waters, thus leading to differences in the sensitivity of dissolution rates to solution chemistry. As can be seen in the table for the low and high pH J-13, U dissolution was less sensitive to pH changes than aluminum. The order of aggressiveness in increasing severity for each element were as follows: for U, high Cl<nominal<high pH<low pH; for Al, high Cl≈nominal<low pH<high pH. From the available data, a temperature change of 25 to 90 °C increased the dissolution rates. The rates did not increase as much in the low pH J-13. Some long-term flow tests are continuing which may further define the effect of temperature.

Table 4. Average Uranium and Aluminum Dissolution Rates ($mg/m^2/d$) from Flow Tests*

		25 °C				90 °C			
Alloy/	Water	Uranium		Aluminum		Uranium		Aluminum	
Fabricat.	Chemistry	Mean	σ	Mean	σ	Mean	σ	Mean	σ
13.2/cast	J-13	1.7	0.9	BD	BD	24.2	53.8	225	228
13.2/wrt		ND	ND	ND	ND	8.2	5.6	102	120
25/cast		ND	ND	ND	ND	26.9	27.7	120	121
19/wrt		2.2	0.8	BD	BD	ND	ND	ND	ND
13.2/cast	Low pH	139	78	1110	544	215	120	1350	699
13.2/wrt		ND	ND	ND	ND	188	115	1110	501
25/cast		227	111	973	544	420	444	1333	712
13.2/cast	High pH	ND	ND	ND	ND	86	57	5250	3045
13.2/wrt		ND	ND	ND	ND	248	210	5440	2731
25/cast		ND	ND	ND	ND	96	105	4710	2034
13.2/cast	High Cl	1.4	0.6	BD	BD	18	9	198	143
13.2/wrt		ND	ND	ND	ND	8.4	3.9	157	163
25/wrt		2.6	3.0	BD	BD	14	7.0	134	97

* ND indicates that data were not measured for this condition. BD indicates that the measured value is below the detectable limit of the technique.

The trends of the U and Al dissolution rates, which are shown in Figures 10-13, were dependent on both solution chemistry and temperature. The dissolution rates shown in the figures was based on the geometric surface area of the sample. Figure 10 shows the U dissolution rates at 90 °C for the 13.2 UAl cast coupons in the different J-13 waters. The other alloys had similar trend curves. As can be seen in the figure, the uranium dissolution was high initially and then decreases. Especially for the more aggressive solutions of high and low pH, rate increases were observed near the end of the test. Even with these perturbations, the dissolution rates of uranium were found generally to have similar trends as reported for commercial nuclear fuel [1,2]. As shown in Figure 11, aluminum also had high initial rates that dropped off. Increases in rates were not observed later in the test. The high pH data was not shown because the values were much larger than the other waters. At 25 °C the trends differ with rates increasing later in the test period or remaining constant for most of the test period. Figure 12 shows the U dissolution rates at 25 °C for the different solutions. The aluminum rates in the low pH J-13 were more variable for the 13.2 and 25 UAl alloys as shown in Figure 13.

The concentration of aluminum ions in the water followed a similar trend to the uranium profiles, peaking initially then decreasing to a lower value. This trend was also observed for the high pH solution in contrast

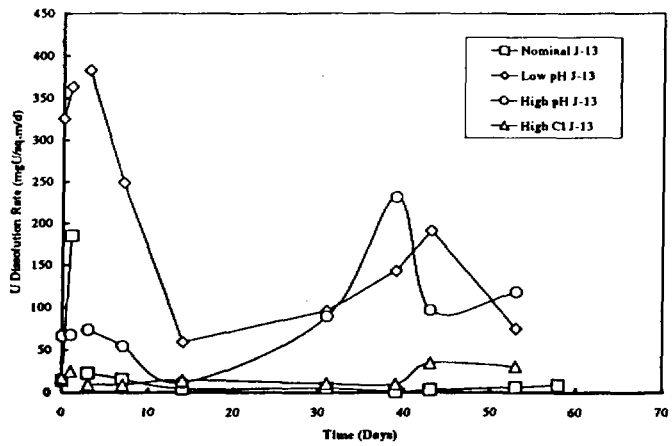

Figure 10. U Dissolution Rates for 13.2 UAl Cast Coupons in J-13 Waters at 90 °C

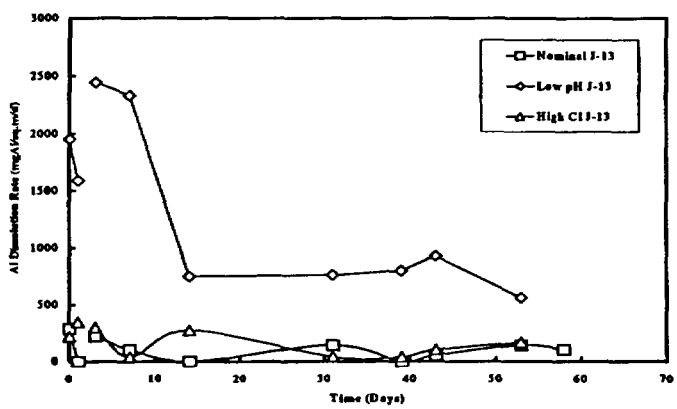

Figure 11. Al dissolution Rates for 13.2 UAl Cast Coupons in J-13 Waters at 90 °C

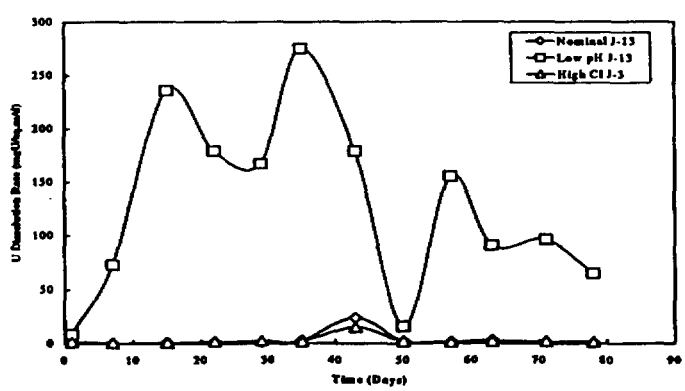

Figure 12. U Dissolution Rates for 13.2 UAl Cast Coupons in J-13 Waters at 25 °C

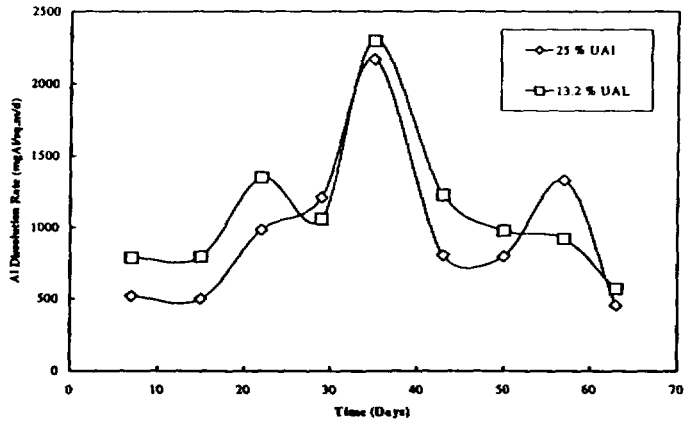

Figure 13. Al Dissolution Rates for 13.2 and 25 UAl Cast Coupons in Low pH J-13 at 25 °C

to the uranium concentration. The aluminum concentrations were lowest in the nominal and high Cl J-13 averaging at about 1 ppm, Peak values, however, differed; the peaks were approximately 2 and 12 ppm for nominal and high Cl J-13, respectively. For the low pH solutions, the average and peak concentrations were ~5 ppm and 13 ppm, respectively. For the high pH solutions, the average and peak concentrations were 20 ppm and 60 ppm, respectively. The higher rates in the high pH J-13 corresponds to the lack of significant oxide formation on the U-Al samples.

At 90 °C the alloys exposed to nominal J-13, 13.2 UAl (cast and wrought) and 25 UAl (cast), had variable surface characteristics. The surfaces generally darkened although spotty regions of shiny metal remained after 13 weeks. Various amounts of white corrosion products and surface roughening were observed. The 25 UAl alloy had the most uniform surface. In low pH J-13, the surfaces were smooth, were covered with a thin brown/white oxide layer which was mottled, and had minimal voluminous corrosion products. In contrast to the nominal J-13 results, the 25 UAl alloy had the most variable surface morphology. The U-Al alloys exposed to the high pH J-13 had a heavy layer of corrosion products which covered a darkened, smooth appearing surface. The 13.2 UAl alloy had the fewest corrosion products. In high Cl J-13, the surfaces had many localized spots of voluminous white corrosion products. The remainder of the surface had a dark and rough appearance. In this water, the 13.2 UAl alloy had the most corrosion products.

The 25 UAl samples from the nominal and low pH J-13 were also examined under high magnification using the SEM. The surfaces were observed both planar and in cross-section. The shiny regions observed visually were found to be areas not covered by oxide or corrosion product, but were active corrosion sites where aluminum corroded preferentially to the U-Al phases as shown in Figure 14. The oxides were primarily aluminum oxide, but also contained sulfur, uranium, and silicon. Calcium compounds, which are also seen in the photomicrograph, were also found to occur regularly on the surface. In the low pH J-13, the samples were found to form an aluminum oxide which uniformly covered the surface, as shown in Figure 15. The surface smoothness noted macroscopically was probably related to the formation of this oxide. The relief of the U-Al particles resulted from the preferential corrosion of the aluminum. Similar to the nominal J-13, the deposits that did form on the surface were calcium compounds.

The degradation at 25 °C was not as severe as at the higher temperature. In the nominal J-13, the surfaces varied from shiny metallic to a dulled, light etch appearance. Some areas were covered with a powdery white corrosion product. In the low pH J-13, the surfaces had a dull, flat appearance with minimal white deposits. Voids in the 25 UAl were readily apparent, although none were seen for the 13.2 UAl. The

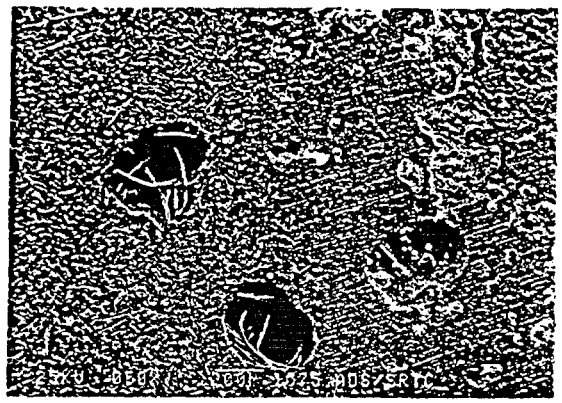

Figure 14. Planar View of Surface Of 25 UAl Cast In Nominal J-13

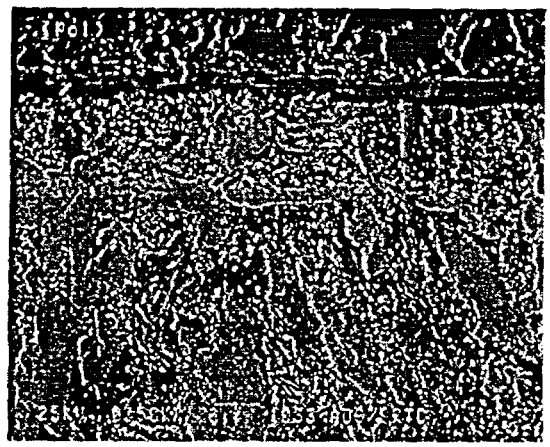

Figure 15. Cross-section of 25 UAl Cast in Low pH J-13

appearances of the coupons from the high Cl J-13 were similar to those for nominal J-13. Some areas had a significant build up of white corrosion products.

The weight changes for the samples were also measured for the 90 °C coupons as shown in Table 5. In general, the 13.2 UAl cast samples had the smallest weight changes which is an indication that the alloy was the least reactive. As reported for the dissolution rates, the weight changes were dependent on the solution chemistry. Weight losses were generally observed in both the low and high pH J-13 with larger weight losses in the high pH J-13 where solubility of aluminum is greater. The samples in the high Cl and nominal J-13 experienced weight gains, with larger gains in the high Cl J-13, attributed to the voluminous corrosion products.

Table 5. Weight Changes of U-Al Alloys in J-13 Well Water*

Type of J-13 Water	Alloy Composition (wt % U)		
	13.2 wrought	13.2 cast	25 cast
Nominal	-0.0039	-0.0007	-0.0024
Low pH	+0.0139	+0.006	+0.0117
High pH	+0.0255	+0.0128	+0.0342
High Cl	-0.0054	-0.0082	-0.007

* A negative number indicates a weight gain, while a positive number indicates a weight loss.

Static Test Results

The overall degradation that occurred during the static tests was minor with the majority of the corrosion occurring on the sides of the coupon rather than the bottom crevice area. However, there were changes in the appearance of the coupons that depended primarily upon the test environment. These changes were unaffected by the composition of the material or its fabrication method. Coupling the coupons to stainless steel increased the severity of attack for a given test solution, as did increasing the temperature of the environment. Concentrations of dissolved uranium and aluminum were in agreement with the observed degradation of the coupon. Although relatively small changes in the weights of the coupons were measured, general trends were in agreement with the observed degradation.

Corrosion Mechanism of U-Al Alloys

Coupons immersed in nominal J-13 visually showed only slight evidence of degradation with only a few white corrosion products indicative of pitting of the aluminum matrix. Figure 16 shows the degraded microstructure of a 13.2 UAl cast coupon that was exposed to nominal J-13. Original grinding marks are seen on the aluminum surface indicating that minimal general corrosion occurred. However, the aluminum matrix adjacent to the U-Al eutectic has been preferentially corroded leaving the particles in relief. The micrograph also shows evidence that eutectic particles became dislodged from the surface. Figure 17 shows loosened U-Al particulate that was collected from a filtered solution. Evidence of these particles was observed from all test solutions.

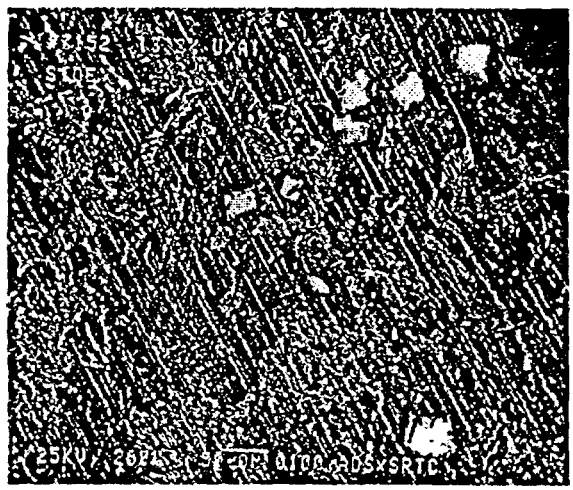

Figure 16. Post-test Microstructure of 13.2 UAl Cast from Nominal J-13 at 90°C

In low pH J-13, a whitish film was observed on the surface of the coupon with no associated white deposits. Figure 18 shows the surface of a 13.2 UAl cast coupon that was immersed in low pH J-13. A thick oxide film covered the surface indicating a more general form of attack. The oxide contained many cracks and fissures and many U-Al particles were embedded in the film. Figure 19 shows a cross-sectional view of the same coupon. As in the case of nominal J-13, the aluminum adjacent to the UAl_4 eutectic particles corroded preferentially. This preferential dissolution of the aluminum matrix led to the particles dislodging and either falling out or becoming embedded in the oxide film.

Exposure of the coupons to high Cl J-13 resulted in the coupon becoming black with numerous white corrosion products indicative of pitting. Figure 20 shows the surface of a 13.2 UAl cast coupon that was immersed in high Cl J-13. As with the nominal J-13, minimal general attack of the aluminum surface was observed however preferential attack of the aluminum matrix occurred next to the U-Al particles. Pitting of the aluminum matrix was more severe than with the nominal J-13. Several large volcanic-like aluminum oxide formations were observed on the surface.

Figure 17. SEM Micrograph of Dislodged U-Al Particles from 25 UAl wrought in High pH J-13 at 90°C

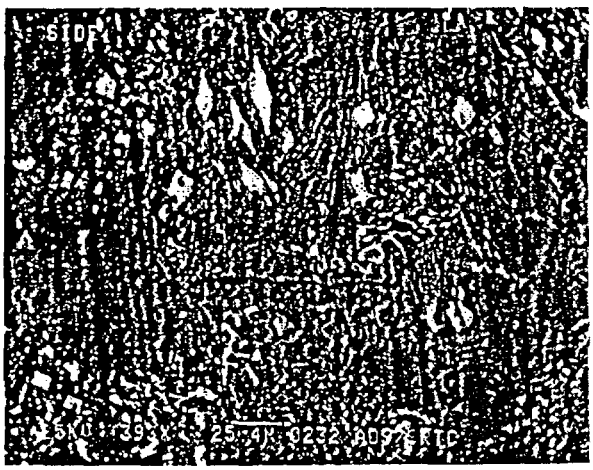

Figure 18. Post-test Microstructure of 13.2 UAl Cast from Low pH J-13 at 90°C

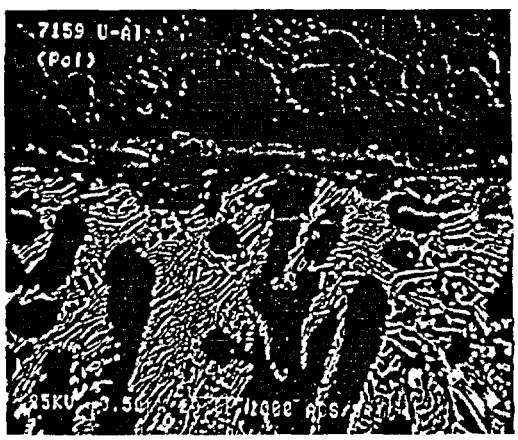

Figure 19. Cross-sectional View of Post-test Microstructure of 13.2 UAl Cast from Low pH J-13 at 90°C

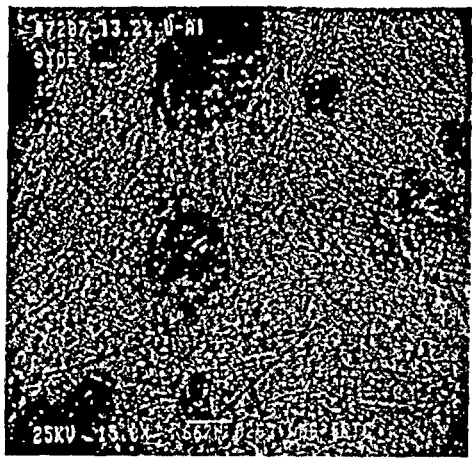

Figure 20. Post-test Microstructure of 13.2 UAl Cast from High Cl J-13 at 90°C

The high pH J-13 resulted in the coupon becoming dark with no white deposits on the coupon. Figure 21 shows the degraded microstructure of the 13.2 UAl cast coupon that was exposed to the high pH J-13. Large, skeletal-like regions of the eutectic remained after the aluminum preferentially corroded. In contrast to the low pH J-13, there was no oxide film present on the surface. The general attack of the aluminum was the most severe of all the test solutions.

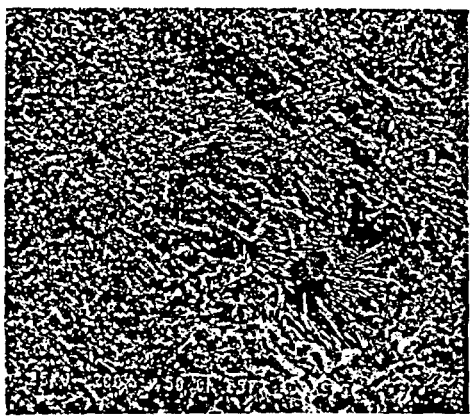

Figure 21. Post-test Microstructure of 13.2 UAl Cast from High pH J-13 at 90°C

As mentioned previously, depending on the uranium concentration the U-Al particles consisted of two possible phases, UAl_3 and UAl_4, each with a distinct microstructure. The 10 UAl coupons consisted of primary aluminum and the eutectic UAl_4 phase. The degradation of the microstructure was the same as that observed for the 13.2 UAl. The 25 UAl coupons on the other hand consisted of both U-Al phases. Figure 22 shows a cross-sectional view of a 25 UAl cast coupon, which contained both phases, from the test in nominal J-13 at 90°C. As with the UAl_4 phase, preferential corrosion of the aluminum matrix occurred around the blocky UAl_3 particles. The aluminum corroded beneath the particle followed by the formation of aluminum oxide that created pressure on the UAl_3 particle. As a result the particle cracked and began to spall from the surface. Thus, both UAl_3 and UAl_4 can be dislodged from the aluminum matrix without significant degradation of the particle. Thus, under these various test conditions the alloys within this composition range had similar corrosion mechanisms. The effect of alloy composition on the dissolution rate should be similar.

Although the fabrication process of the material affected the microstructural features, the corrosion mechanism was not affected. Figure 23 shows a cross-sectional view of a 13.2 UAl wrought coupon that had been immersed in low pH J-13 at 90 °C. As was observed with the 13.2 UAl cast coupons, the aluminum matrix has preferentially corroded and the U-Al particles have become embedded in the oxide. The only difference is that the sizes of the particles that are dislodged from the surface of the wrought material are smaller than those that are released from the cast material. The release of these small U-Al particles should only have a small impact on the dissolution rates of the radionuclides, since the rates in J-13, as discussed previously, were very low.

Figure 22. Cross-sectional View of Post-test Microstructure of 25 UAl Cast from Nominal J-13 at 90°C

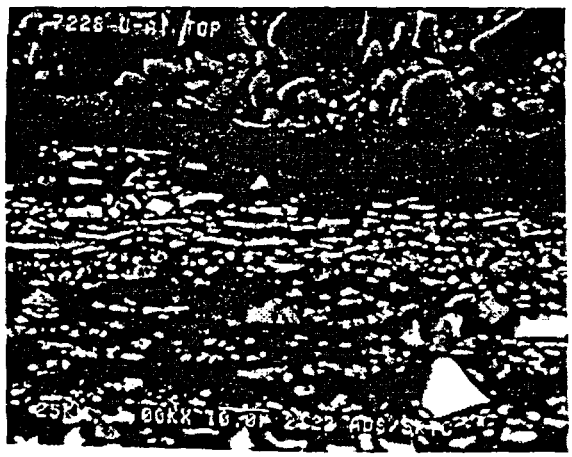

Figure 23. Cross-sectional View of Post-test Microstructure of 13.2 UAl Wrought from Low pH J-13 at 90°C

The type of galvanic couple and the temperature of the environment affected the severity of attack. For example, in the high Cl J-13 the number of pits was much greater for coupons attached to the stainless steel disk than to the aluminum disk (see Figure 24). Increasing temperature also increased the severity of attack. At 25°C in the high Cl and high pH J-13, the number of pits was significantly less than at 90°C. The number of deposits on the surface was less at the lower temperature than at the higher, although the deposits were more voluminous than at the higher temperature. This result probably reflects the lower solubility of the aluminum oxide at the lower temperature.

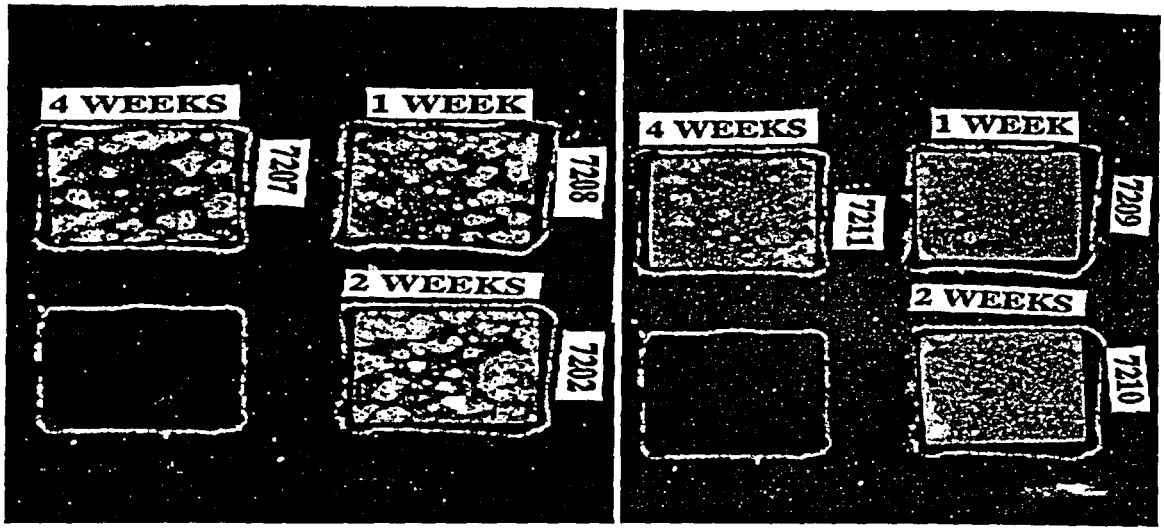

(a) (b)

Figure 24. Visual Appearance of 13.2 UAl Cast from High Cl J-13 at 90°C and Coupled to a) Stainless Steel and b) Aluminum (2X)

The crevice area of the coupons demonstrated little evidence of attack. The primary site of degradation was near the edge of the coupon. Figure 25 shows a typical crevice surface with a relatively thick oxide that contained striations. These markings were similar to the grinding marks from the stainless steel and aluminum disks as shown in the figure. Areas where this oxide had cracked and spalled were observed intermittently. Preferential dissolution of the aluminum was also seen at these local areas.

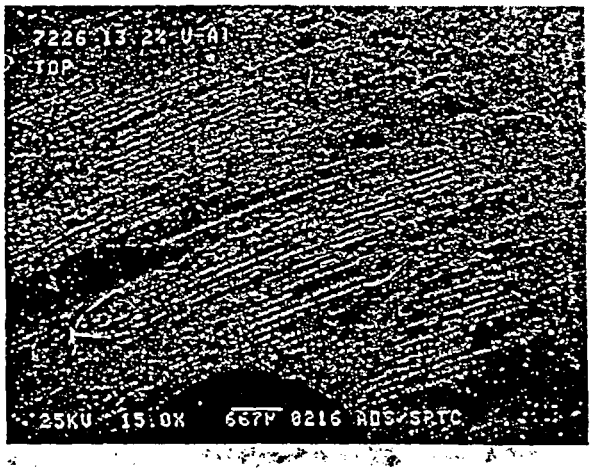

Figure 25. Post-test Surface of Crevice Area of 13.2 UAl Wrought from Nominal J-13 at 90°C

Analysis of Test Solutions Dissolved Species

Table 6 shows the dissolved uranium concentration for static tests at 90°C as a function of test solution, galvanic couple, and alloy composition. The test solution had the most significant effect on the amount of uranium dissolved. For each galvanic couple the relative severity of the solution was similar. For the stainless steel, the amount of dissolved uranium increased in the following order: high Cl < nominal < low pH < high pH J-13 with a ratio of 1:2:4:10. For the aluminum, the amount of dissolved uranium increased in the following order: high Cl, nominal < low pH < high pH J-13 with a ratio of 1:10:20. The amount of uranium dissolved in each of these solutions was in agreement with the severity of degradation that was

observed on the coupons. The high pH and low pH J-13 were the most aggressive environments while the chloride and nominal were the least aggressive.

The galvanic couple affected the severity of attack. The amount of uranium dissolved was 2 to 10 times greater in solutions with coupons attached to the stainless steel than with coupons coupled to the aluminum. This result is in agreement with the observations that the coupons attached to the stainless steel showed more evidence of degradation.

No effects of alloy composition or fabrication on the uranium dissolution were apparent. In general, the amount of dissolved uranium was constant for the different alloys. This result was consistent with the result that the primary degradation mechanism was unaffected by alloy composition or fabrication technique.

Table 6. Concentration (ppm) of Dissolved Uranium in Static Tests at 90°C: a) Stainless Steel and b) Aluminum

a) Stainless Steel

Solution	10 UAl cast	13.2 UAl cast	13.2 UAl wrought	25 UAl cast	25 UAl wrought
J-13	0.2-0.8	0.6-0.7	0.5-0.6	0.5-0.6	0.6-0.7
Low pH	0.5-0.6	2.5	2-2.5	1-2	2.5-3
High Cl^-	0.2	0.25-0.3	0.2-0.25	0.25-0.4	0.3
High pH	1-4	3.5-4.5	1-1.2	3-4	15-20

b) Aluminum

Solution	13.2 UAl cast	13.2 UAl wrought	25 UAl cast	25 UAl wrought
J-13	0.05	0.05	0.1	0.05-0.2
Low pH	1-1.5	0.5-0.8	0.25-0.75	0.9-1
High Cl^-	0.05	N/A	0.08-0.1	0.1
High pH	0.1	N/A	2	1.2-1.4

Table 7 shows the effect of temperature on the dissolved uranium concentration. The tests were performed on 13.2 UAl cast material coupled to stainless steel. For coupons tested in nominal, high Cl, and low pH J-13 the amount of dissolved uranium increased by a factor of 3 to 10 as the temperature increased from 25 °C to 90 °C. The coupons tested in the high pH J-13 showed an even stronger dependence on temperature as the dissolved uranium concentration increased by a factor of 100. These results agree with the observations that the severity of attack increased with temperature.

Table 7. Concentration (ppm) of Dissolved Uranium for 13.2 UAl Cast Material Couple to Stainless Steel in Static Tests as a Function of Temperature

Solution	25 °C	90 °C
J-13	0.05-0.09	0.6-0.7
Low pH	0.5-0.7	2.5
High Cl	0.08-0.13	0.25-0.3
High pH	0.03	3.5-4.5

The dissolved aluminum concentration was also analyzed for the static tests and the results for tests at 90 °C are shown in Table 8. The effect of solution composition on the dissolved aluminum concentration was slightly different than for the dissolved uranium concentration. The nominal, high Cl, and low pH J-13 dissolved relatively the same amount of aluminum. The high pH J-13, however, dissolved 5-10 times more than the other solutions. This result correlates with the higher solubility of aluminum in alkaline solutions

[8]. The other observed effect was that for the low pH J-13 a maximum dissolved aluminum concentration was achieved after 1 week. The decrease was likely due to precipitation of an aluminum oxide film. This mechanism is in agreement with the thick oxide that formed on the coupons that were immersed in the low pH J-13.

The galvanic couple affected the dissolved aluminum concentration differently than the dissolved uranium. For three of the solutions, nominal, high Cl, and high pH J-13, the tests with the aluminum plate produced a greater dissolved aluminum concentration than those with the stainless steel. This result probably reflects the corrosion and dissolution of additional aluminum from the plate. On the other hand coupons exposed to the low pH J-13 and coupled to stainless steel resulted in the higher dissolved aluminum concentration. This result likely was due to the formation of the aluminum oxide on both the plate and the coupon.

As with the dissolved uranium concentration, no effects of alloy composition or fabrication on the dissolved aluminum concentration were apparent. With only a couple of exceptions the amount of dissolved aluminum was constant for a given galvanic couple and test solution.

Table 8. Concentration (ppm) of Dissolved Aluminum in Static Tests at 90 °C: a) Stainless Steel and b) Aluminum

a) Stainless Steel

Solution	10 UAl cast	13.2 UAl cast	13.2 UAl wrought	25 UAl cast	25 UAl wrought
J-13	2-2.5	2-3	1.5-2	2.5-4	2.8-3
Low pH	1-5	4-9	5.5-11.8	1-3	3.2-12.5
High Cl^-	2.1-4.4	3.5-6.2	1-4	2.2-9.6	2.8-4.5
High pH	91-114	36-40	1-8	11-15	50-63

b) Aluminum*

Solution	13.2 UAl cast	13.2 UAl wrought	25 UAl cast	25 UAl wrought
J-13	5-6.5	5-5.5	2.5-4	3.1-3.7
Low pH	3.5-6	2-4.5	0.5-4	3-7.8
High Cl^-	8-15	N/A	2.5-4.2	2.1-3.5
High pH	63-80	N/A	12-13	113-138

* N/A – not available

Table 9 shows the effects of temperature on the dissolved aluminum concentration. The tests were performed on 13.2 UAl cast material coupled to stainless steel. For nominal and high Cl J-13 the dissolved aluminum concentration increased by a factor of 10 as the temperature increased from 25 °C to 90 °C, while for the high pH J-13 the dissolved aluminum increased by a factor of 100. These increases were about the same order of magnitude as those observed for the dissolved uranium. For the low pH J-13, on the other hand, the amount of dissolved aluminum was not affected by temperature, while the dissolved uranium concentration increased by a factor of 3 to 5. The same maximum value of dissolved aluminum after one week that was observed for the tests at 90 °C also occurred at the lower temperature. Evidently the precipitation of the aluminum in the low pH J-13 is insensitive to temperatures within this range.

Table 9. Concentration (ppm) of Dissolved Aluminum for 13.2 UAl Cast Material Coupled to Stainless Steel in Static Tests as a Function of Temperature

Solution	25°C	90°C
J-13	0.25	2-3
Low pH	4-7.4	4-9
High Cl^-	0.25	3.5-6.2
High pH	0.25	36-40

Corrosion Losses of U-Al Alloys

As mentioned above, the weight change in the coupons after 1 month were small, which may hide variable effects. Table 10 shows the weight changes for tests performed at 90°C. Both weight gains and weight losses were observed for the tests. Although there were some inconsistencies in whether a weight loss or gain was observed, some generalizations with regard to the magnitude of the weight change were apparent. Test solution had a significant effect on the weight change. The weight changes observed for coupons from the low pH and high pH J-13 tests were approximately 6-7 times greater than those from the nominal and high Cl J-13. This result is in agreement with the measurements of dissolved species and the observed degradation. Effects due to the galvanic couple were also observed. The weight changes for coupons attached to the stainless steel were 2-5 times greater than that of coupons attached to the aluminum. As before there were no apparent effects on the weight change due to either alloy composition or fabrication.

Table 10. Weight Changes ($\mu g/dm^2$) in Coupons from Static Tests of 13.2 UAl Cast at 90°C for Stainless Steel and Aluminum Galvanic Couples

Solution	**Stainless Steel**	**Aluminum**
J-13	-1000 to -6000	200 to 900
Low pH	-10000 to 43000	0 to 13000
High Cl^-	2000 to 5000	0 to 2200
High pH	-25000 to -36000	-4000 to -2500

The weight change as a function of temperature is shown in Table 11. The trend of greater weight change with increased temperature was not observed in some cases. As expected the weight change in the high pH J-13 was a factor of 10 greater at 90°C than at 25°C. However, for the nominal and low pH J-13 there was little difference in the weight change between the two temperatures and for the high Cl J-13 the magnitude of the weight change at the lower temperature was actually greater. This result appears to be consistent with the large, voluminous corrosion products. Clearly, the measurement of weight change was not as strongly correlated to temperature as the concentration of dissolved species.

Table 11. Weight Changes ($\mu g/dm^2$) in 13.2 UAl Cast Coupons Coupled to Stainless Steel in Static Tests as a Function of Temperature

Solution	25 °C	90 °C
J-13	500 to -5500	-1000 to -6000
Low pH	-5000 to -30000	-10000 to 43000
High Cl^-	-100 to -22000	2000 to 5000
High pH	-100 to 2000	-25000 to -36000

Electrochemical Test Results

For the electrochemical test, the corrosion behavior of Al-SNF was characterized as a function of water chemistry, alloy composition, and temperature. The corrosion behavior and polarization characteristics for the three tested alloys, 10, 13.2, and 25 UAl, were similar. The alloys were taken from cast ingots only. The

variable effects were evaluated for the corrosion potential, the linear polarization resistance, and the characteristics of the polarization scan (the potential-current plot). A corrosion rate (CR) was calculated from the linear polarization resistance (R_P) based on the density (ρ) and equivalent weight (EW) of aluminum,

$$CR = K \times EW / R_P \times A \times \rho ,$$

where K is a constant and A is the surface area.

The polarization curves displayed two different patterns indicative of changes in the corrosion characteristics. The results were a function of both water chemistry and temperature. The primary degradation mechanism was low general corrosion accompanied by some degree of pitting. The pitting was dependent on the chloride concentration. The corresponding cyclic polarization curve is shown in Figure 26 for a 13.2 UAl sample in nominal J-13 at 90°C. Note that the magnitude of the reverse current is larger than the current during the forward scan. This hystersis means the material is susceptible to pitting [9]. In the high pH J-13, the alloys underwent general corrosion as shown by the polarization curve in Figure 27 for 10 UAl in high pH J-13 at 25°C.

The UAl alloys in low pH J-13 at 90 °C also showed an oxide-induced passivity which was susceptible to pitting. This passivity attributed to the more noble potential of the alloys. A pitting potential was found to be at –0.2 V where an increase in current occurred due to pitting. The UAl alloys grew a thick oxide/corrosion product layer during exposure as shown in Figure 18 from the static test. In the other waters, these layers were either not observed or not as thick. For the other conditions in which pitting was observed, the alloys probably did not manifest a pitting potential since their corrosion potentials were near or above the pitting potential.

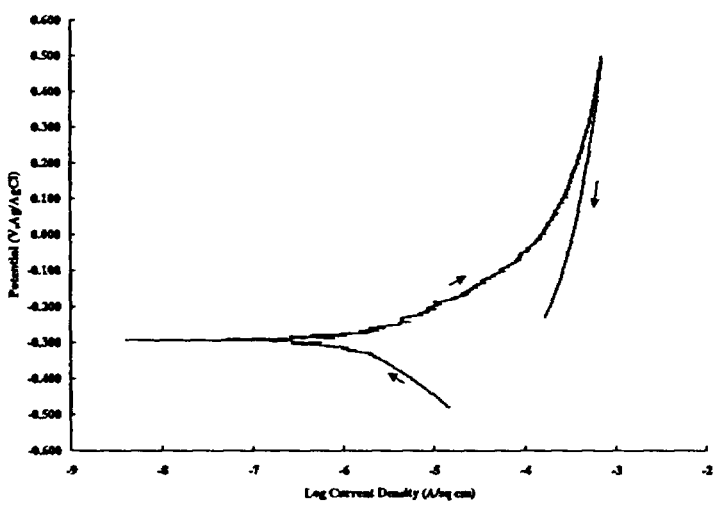

Figure 26. The Polarization Curve for 13.2 UAl in Nominal J-13 at 90 °C

The other electrochemical parameters, corrosion potential and corrosion rate, are given in Table 12 as a function of the test variables. For any given water chemistry and temperature, the corrosion potentials of the alloys were similar with those in the high pH J-13 being the most active in a range of –1.2 to –1.5 V. The corrosion potentials of the alloys in the nominal and high Cl J-13 waters were fairly similar, typically -0.3 to -0.53 V. The corrosion potentials in the low pH J-13 were the most noble, -0.25 to -0.46 V. Active potentials are indicative of alloys with a lower corrosion resistance relative to noble potentials. The potentials of the alloys became more active, that is more electronegative, with an increase in temperature in the nominal and high Cl waters. In the low and high pH J-13, the potentials became more noble which

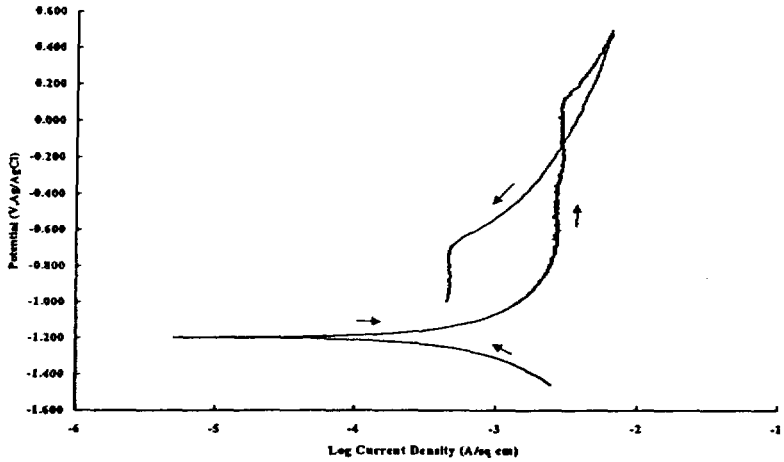

Figure 27. The Polarization Curve for 10 UAl in High pH J-13 at 25 °C

indicated a difference in the corrosion characteristics of Al-SNF. This potential shift for the low pH was not always steady but at times fluctuated between passive and active values indicating an unstable oxide or partial coverage by the oxide.

Table 12. Corrosion Potentials and Rates for Cast U-Al Alloys in J-13 Waters

Corrosion Potential (V)

Alloy	Temp (°C)	J-13	Low pH	High pH	High Cl
10	25	-0.385	-0.505	-1.525	-0.460
	90	-0.450	-0.260/ -0.320	-1.22	-0.530
13.2	25	-0.295	-0.275/ -0.480	-1.470	-0.460
	90	-0.375	-0.330	-1.190	-0.825
25	25	-0.460	-0.400	-1.510	-0.480
	90	-0.450	-0.340	-1.225	-0.530

Corrosion Rate (mpy)

Alloy	Temp (°C)	J-13	Low pH	High pH	High Cl
10	25	1	3	56	1.5
	90	6	2.25	50	2.4
13.2	25	0.6	0.1/2.1	60	0.8
	90	3.4	3.7	59	1.0
25	25	0.5	2	58	1.3
	90	6	3.5	50	4.9

The corrosion rates of the alloys were similar for the J-13 waters at a given temperature as indicated in Table 12. The rates in the high pH J-13 were the largest at approximately 60 mpy, which corresponded to the most active corrosion potentials. The rates in the other waters were all similar ranging from 1-6 mpy. Changing temperature affected the corrosion rates in the waters with the low corrosion rates. However, the corrosion rate in the high pH J-13 surprisingly was unaffected. The increased corrosion rate occurred with a shift to more active corrosion potentials as discussed above.

From macroscopic observations, the corrosion morphologies of the alloys after the polarization tests were similar and dependent on the J-13 water chemistry. In the nominal J-13, the surface had a smooth, mottled appearance of light and dark regions. The surfaces appeared to be pitted at 25 °C, whereas at 90 °C the overall surface was rougher indicating the higher corrosion rate. White corrosion deposits were observed near pits or voids. The morphology resulting from exposure to the low pH J-13 at 90 °C appeared flat with a dark tarnished appearance and random white deposits. At 25 °C, the surface was not darkened and fewer

corrosion products were observed. Corrosion product formation and surface roughness was greater in the high pH J-13 which indicated the higher corrosion rate than in the other waters. Voluminous, volcanic-like deposits covered a dark surface. The corrosion products that formed in high Cl J-13 formed a more uniform surface layer with fewer discrete deposits. Surface roughening appeared minimal, although pits were numerous as expected.

IV. DISCUSSION

Uranium Dissolution Rates and Radionuclide Release Rates

The preliminary U dissolution rates from Al-SNF were found to have only a small dependence on the fuel composition, but depended more significantly on the environmental conditions. As can be seen in Table 3, the rates for each solution were in a close range for each solution chemistry, except for the U-Al fuel in the nitric solution. These data, although preliminary, support a singular model to assess Al-SNF for repository storage. The preliminary results for the other radionuclides, however, showed greater variability, especially for Tc which has a long decay time. The causes of this variability as yet are unknown. Most of the other radionuclides had trends and dissolution rates that were comparable to that of uranium. Although the preliminary data characterize the Al-SNF dissolution characteristics, further testing is required to improve the confidence level for any model chosen to determine the impact of these characteristics on repository storage.

The test results on unirradiated U-Al alloys, which simulate the Al-SNF, were found to be in good agreement for the general dissolution characteristics of the irradiated fuel, especially in the J-13 and bicarbonate solutions. In these two solutions, the U dissolution rates fall within the range of the irradiated fuels. In the nitric acid solution, the rate was significantly higher and resulted from attack of the U-Al particles as was shown in Figure 19 (c). The dissolution rate for the 19 UAl is similar to that measured for the 13.2 and 25 UAl in other unirradiated alloys. The high U dissolution rate in these alloys is attributed to partial oxidation as described below. The irradiated fuels may have formed a more tenacious oxide resulting in lower dissolution rates. The oxidation characteristics of irradiated and unirradiated fuels may differ. The difference in U dissolution rates among the unirradiated fuels in J-13 is also an anomaly.

Effect of Degradation Mechanism on the Uranium Dissolution Rate

Degradation Mechanism

Each test method produced similar degradation of the unirradiated UAl alloys for a given test environment, alloy composition, or fabrication. The primary degradation characteristic was that the aluminum matrix corroded preferentially to the U-Al particles. A micro-galvanic cell was established between the aluminum and the U-Al particles with the attack of the aluminum being most severe in the region adjacent to the particle or in between eutectic lamellae. As a result of this preferential corrosion, many of the particles became dislodged from the surface. The presence of the particle in the solution depended on whether or not an oxide film formed to entrap the particle.

Degradation of the U-Al particles was not observed in the studies at SRS and only observed in the nitric acid tests at PNNL. For the SRS studies, however, the dissolved uranium concentration was greater than that expected from the uranium present in the aluminum matrix alone. Therefore, it seems likely that uniform corrosion of the particle occurred. It is uncertain whether this attack occurred while the particle was part of the aluminum matrix or after it had become dislodged.

The heterogeneity of the surface microstructure likely played a role in the variability of the data. The heterogeneity manifested itself in two ways: a) the area fraction of U-Al particles and b) the formation of a non-uniform aluminum oxide film. Depending on which microstructural features are exposed initially, the area fraction of the U-Al particles exposed to the environment during the tests could be quite different. A large area fraction of the cathodic U-Al particles would enhance the dissolution of aluminum and the possibility that a number of particles would be dislodged. The presence of an oxide film would retard the

degradation of the aluminum except in localized areas where film breakdown occurs. The presence of the particles in the aluminum matrix may create a strain in the oxide film and result in mechanically weak sites in the oxide film. The distribution of these sites again would be variable.

The degradation mechanism for irradiated fuels is expected to be similar to that of the unirradiated data and will be assessed after post-test characterization is completed. The known microstructural differences, such as fuel type (U_3O_8, U_3Si_2, etc) and particle coarsening in irradiated fuels, may cause minor variations, but is not expected to affect the overall dissolution rate of radionuclides. However, the degradation of Al-SNF is a significant factor in understanding the dissolution and redistribution of the radionuclides in these fuels.

Effects of Environmental Variables on the Dissolution and Degradation of Al-SNF

The solution composition was found to have the most significant effect on dissolution, degradation, and formation of corrosion products. The severity of attack generally increased in the following order: nominal, high Cl < low pH < high pH J-13.

The nominal and high Cl J-13 were at a pH where a protective oxide forms on aluminum [8]. Thus the general attack was minimal, although pitting attack was observed. As expected the pitting attack in the high Cl J-13 was greater than in nominal J-13. In addition, the dissolved aluminum concentration was generally higher for the high Cl J-13. However, the dissolved uranium concentrations were nearly the same or slightly lower in high Cl J-13 compared to the nominal J-13. Evidently, the dissolution of uranium was not affected by the presence of chloride at these levels.

The low pH J-13 was at pH levels where general attack of the aluminum matrix occurred with significant degradation of the U-Al particles. The thick oxide film produced in the low pH J-13 was the result of precipitation on the surface. A mechanism would involve an initial rapid corrosion and dissolution of aluminum and uranium from both the particulate and the matrix. Al dissolution would also result in the removal of the U-Al particulate from the matrix. In the flow tests under unsaturated conditions, this type of degradation led to the high U dissolution rates for the low pH J-13. Once the dissolved Al concentration reached saturation, an oxide would precipitate on the surface. The metal surface would then be protected, entrapping U-Al particles in the oxide and slowing further degradation and dissolution. For the flow test, the irregular oxide film allowed U dissolution to proceed, while under saturated conditions in the static tests a thick oxide slowed the U dissolution. Figures 15 and 18 show the condition of the oxide in low pH J-13 for the flow and static tests, respectively. Further investigation into the kinetics and development of the oxide film is necessary to model this dissolution.

In contrast, an oxide film did not form on the surface of coupons immersed in the high pH J-13. In this case, the U-Al particles are continuously exposed to the solution. The measured U concentration and dissolution from the static and flow tests indicated that the U dissolution was slowed. For the static tests, dissolved uranium concentration remained constant after one week, indicating that saturation is reached relatively quick. From a thermodynamics perspective [7], a greater U concentration would be expected in the low pH J-13 due to the higher solubility of uranium as was observed in the flow test. The aluminum concentration continued to increase with time over the duration of the test. For high pH J-13, the Al dissolution rate and concentrations were the largest of the tested solutions in all tests. Further studies on the kinetics would be needed to model the dissolution for a high pH J-13 scenario.

The coupling of the UAl alloys to stainless steel had a significant effect on the severity of attack in the static tests. The stainless steel and aluminum plates both were large cathodic areas relative to the UAl alloys. However, the stainless steel plate accelerated the corrosion of the Al matrix in the alloy samples as compared to the corrosion that occurred when coupled to the aluminum plate. Coupling between the packaging and the fuel, therefore, would accelerate the degradation and the release of the uranium and other radionuclides. A couple between the fuel meat and any remaining aluminum cladding would have less of an impact on the fuel degradation.

The dissolution and degradation of the UAl alloys were also affected by temperature. This effect was greatest for the high pH J-13 in which there is no protective oxide present and the least in the environment where a thick oxide was present (i.e., low pH J-13). Initially aqueous corrosion in the repository will occur at temperatures near the boiling point. However, as the temperature decreases with time the degradation and the amount of radionuclides released will likely decrease unless there is a catastrophic event that increases the temperature.

V. CONCLUSION

Uranium dissolution rates were measured on irradiated Al-SNF specimens by the single pass flow test. The uranium dissolution rates were insensitive to the type of fuel, but showed a strong dependence on the test environment. The most aggressive environment was the nitric acid solution (30-100 $mgU/m^2/d$), while the least aggressive was the nominal J-13 well water (0.14-0.22 $mgU/m^2/d$). Dissolution rates for radionuclides such as Cs, Sr, and Pu were approximately the same as the U dissolution rates over the duration of the test. However, Tc dissolution rates showed a large degree of variability and did not always coincide with the U dissolution rates.

The effect of the degradation mechanism on the U dissolution rate was investigated with several tests. The first stage of the degradation mechanism was consistent in all environments. The aluminum matrix adjacent to the U-Al particles preferentially corroded leaving the particles in relief. Many times the particles became dislodged and were relocated into the solution. At unsaturated conditions the U dissolution rates are highest in the low pH J-13 and lowest in the high Cl J-13. The second stage of the degradation mechanism depended on the environment in which the material was immersed. In the nominal and high Cl J-13, a thin protective oxide film deposits on the surface of the coupon. The coupon was susceptible to pitting of the aluminum matrix at localized sites. The amount of pitting was greatest in the high Cl J-13, however, the dissolution rate of U was insensitive to chloride concentration in the range tested. In low pH J-13 general corrosion of the aluminum occurred. Once the solution became saturated with aluminum, a thick, aluminum oxide precipitated on the surface. Under saturated conditions, this slowed the dissolution of uranium. In high pH J-13 solutions, general dissolution of the aluminum also occurred. However, in this case the aluminum remains dissolved and no oxide forms on the surface and the aluminum continues to corrode. The amount of dissolved U was limited by the solubility of uranium at the high pH. In the saturated tests, the amount of dissolved U was greatest for the high pH J-13.

In addition to solution chemistry, the effects of other experimental variables such as temperature and galvanic coupling on the U dissolution rate were investigated. In solutions where a thin oxide or no oxide formed (i.e., nominal, high Cl, and high pH J-13), the U dissolution rate increased with temperature. However, in cases where a thick oxide (5-10 μm) was formed (i.e., low pH J-13) the U dissolution rate was insensitive to temperature. The stainless steel galvanic couple resulted in an increase in the degradation and dissolution rate in all solutions.

VI. ACKNOWLEDGEMENTS

The authors would like to gratefully acknowledge the assistance of A. L. Williams, K. R. Hicks, A. W. Bowser, and G. J. Cannell. This work was supported by the U. S. Department of Energy under contract No. DE-AC09-96SR18500. The authors also acknowledge the discussions held with W. J. Grey during this work and the use of PNNL data from the irradiated Al-SNF samples.

VII. REFERENCES

1. Gray, W. J. and C. N. Wilson. 1995. Spent Fuel Dissolution Studies: FY 1991 to 1994, PNL-10540. Pacific Northwest National Laboratory, Richland, Washington.

2. W. J. Gray, H. R. Leider, and S. A. Steward. "Parametric Study of LWR Spent Fuel Dissolution Kinetics," Journal of Nuclear Materials, Vol. 190. Pp. 46-52, 1992.

3. W. J. Gray, "Dissolution Rates of Aluminum-Based Spent Fuels Relevant to Geological Disposals," PNNL-11979, 1998.

4. ASTM G31-72, "Standard Practice for Laboratory Immersion Corrosion Testing of Metals," American Society For Testing And Materials, Philadelphia, PA, 1996.

5. ASTM G5-94, "Standard Reference Test Method for Making Potentiostatic and Potentiodynamic Anodic Polarization Measurements," American Society For Testing And Materials, Philadelphia, PA, 1996.

6. ASTM G59-91, "Standard Practice for Conducting Potentiodynamic Polarization Resistance Measurements," American Society For Testing And Materials, Philadelphia, PA, 1996.

7. J. A. Beavers, N. G. Thompson, and C. L. Durr, "Approaches To Life Prediction For High-Level Nuclear Waste Containers In the Tuff Repository," Application of Accelerated Corrosion Tests to Service Life Predicted of Materials, ASTM 1194. G. Cragnolino and N. Sridhar (eds.), American Society for Testing and Materials, Philadelphia, 1994.

8. M. Pourbaix. Atlas of Electrochemical Equilibria in Aqueous Solutions. National Association of Corrosion Engineers. Houston, TX. 1974.

9. David C. Silverman. "Tutorial on Cyclic Potentiodynamic Polarization Technique," Corrosion98, NACE International, Paper No. 299, 1998.

WESTINGHOUSE SAVANNAH RIVER CO. REPORT WSRC-TR-98-00290

DISTRIBUTION

SAVANNAH RIVER SITE

E. R. Conaster, 704-C
M. E. Dupont, 707-C
R. J. Skwarek, 704-C
H. Brooks, 707-C
W. F. Swift, 707-C
S. D. Burke, 707-C
D. Bickley, 707-C
T. J. Worrell, 705-K
C. R. Wolfe, 773-A
T. L. Capeletti, 773-41A
N. C. Iyer, 773-A
M. R. Louthan, 773-A
J. P. Howell, 773-41A
H. B. Peacock, Jr., 773-A
F. C. Rhode, 773-A
T. M. Adams, 773-41A
P. E. Zapp, 773-A
B. Cederdahl, 773-A
J. I. Mickalonis, 773-A
P. S. Lam, 773-41A
B. J. Wiersma, 773-A
W. F. Ayers, 773-41A
R. L. Sindelar, 773-41A
D. W. Vinson, 773-A
DOE-SR (10 copies)/ J. M. Ridley, 707-K
Site Records, 773-52A